Sensing Performance of Wideband Full-Duplex Joint Radar–Communications FM–FSK Transceiver

Jaakko Marin, Micael Bernhardt, and Taneli Riihonen

Faculty of Information Technology and Communication Sciences, Tampere University, Finland
e-mail: jaakko.marin@tuni.fi

***Abstract*—We study through simulations a system of two full-duplex integrated sensing-and-communications transceivers, which embed data onto a frequency-modulated (FM) continuous-wave radar signal through frequency-shift keying (FSK). Each processing receiver has to extract both target and data information while being subject to self- and mutual interference, including radar echoes. We evaluate sensing and communications performance of this setup under ideal conditions as well as under imperfect synchronization, with the focus on sensing. Under these conditions the setup is estimated to be capable of, e.g., detecting a 1 m^2 radar target at 8 km while transferring data at 400 kbit/s.**

***Index Terms*—Full-duplex, integrated sensing and communications, joint radar and communications, frequency-shift keying.**

I. Introduction

The expected surge in the amount of devices and services supporting wireless connectivity and incorporating remote sensing abilities might lead us to a state where spectrum becomes an overly scarce and disputed resource. This may cause situations with extreme congestion and co-channel interference, severely limiting performance of such systems.

Over the last years, integrated sensing and communications (ISAC) has attracted great interest among research groups due to its ability to solve this problem through joint design and implementation of sensing and communication functionalities using the same waveforms [1], [2]. Besides improving efficiency in the use of spectral resources and reducing the interference experienced by receivers, ISAC systems also have the potential to reduce implementation costs by utilizing a dual-purpose hardware and signal processing platform. These systems are expected to emerge in diverse application spheres, such as autonomous vehicles and unmanned aerial vehicles (UAVs), sensing of the environment, indoors positioning, monitoring of human activities, etc. [1], [3].

Depending on the main focus of the waveform design, ISAC systems can be classified either as communication- or sensing-centric, or as joint-waveform designs [4]. The first group refers to systems that exploit traditional data-loaded waveforms to extract information about the surrounding environment. Conversely, sensing-centric devices are based on signals primarily destined to remote sensing tasks, but adapted to also convey information at rather modest data rates. Last, jointly-optimized systems offer an acceptable trade-off between both functions.

This work was supported by the Research Council of Finland under the grant 341489/346622 and the Finnish Scientific Advisory Board for Defence.

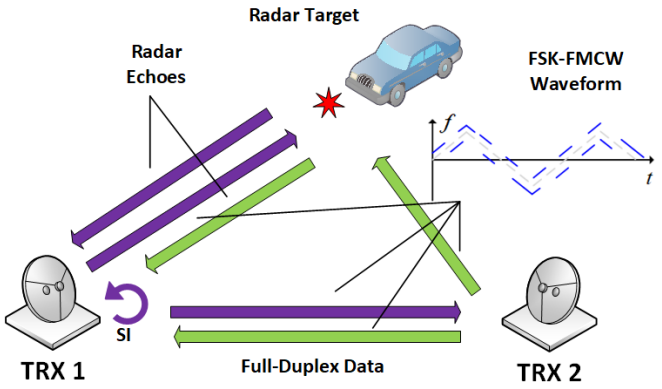

Fig. 1. Concept figure showing a possible use-case scenario and the used waveforms. Radar signals and self-interference are not shown for TRX 2.

Frequency-modulated (FM) waveforms stand out as cost-effective options when implementing sensing-centric systems due to their rather simple implementation and lower hardware requirements. Furthermore, introduction of frequency-shift keying (FSK) on top of an FM continuous-waveform (FMCW) signal has been proposed and investigated before, showing that it can improve sensing performance [5] and increase robustness against electronic countermeasures [6], besides transmitting useful information [7], [8].

Simultaneous transmission and reception, also known as full-duplex (FD), has not been comprehensively studied in the context of ISAC systems. Indeed, the focus in previous publications has been on transmitting information while sensing the environment but without considering simultaneous reception of data signals from secondary transmitters [9], [10].

Herein, we investigate properties of a FD transceiver (TRX) using a sensing-centric FM–FSK waveform that enables ISAC with relatively simple hardware. We proposed this transceiver structure in previous works, for which we simulated data reception and radar performance in a simplistic scenario [11] and conducted experimental measurements showing how well our system would work in a real-world situation [12]. In this paper, we centre our attention mainly on sensing performance of the received echoes under impairments such as interference from another transceiver, which emits a similar signal and whose bits the first one tries to decode, as illustrated in Fig. 1.

II. System Description

A. Signal Models

Without loss of generality, we will present our model and analysis from the perspective of TRX 1 in Fig. 1. The expression for its transmitted signal is

$$s_1(t) = \mathrm{Re}\left\{e^{j2\pi\varphi_1(t)}\right\} = \cos\left(2\pi\varphi_1(t)\right), \tag{1}$$

$$\varphi_1(t) = f_{\mathrm{C}}t + \int_0^t f_{\mathrm{W}}(\theta)d\theta + \int_0^t f_{\mathrm{M}}(\theta)d\theta. \tag{2}$$

Here f_{C} is the carrier frequency, and $\varphi_1(t)$ is defined using integrals to guarantee continuous phase and reduce spectral leakage in the transmitted signal. The first integrated function in (2) is the instantaneous frequency $f_{\mathrm{W}}(t)$, which we set as a triangular frequency-sweeping waveform defined as follows

$$f_{\mathrm{W}}(t) = \begin{cases} -\frac{B_{\mathrm{B}}}{2} + \rho\left(t - mT_{\mathrm{B}}\right), & m \le \frac{t}{T_{\mathrm{B}}} < m+\frac{1}{2}, \\ \frac{B_{\mathrm{B}}}{2} - \rho\left[t - \left(m+\frac{1}{2}\right)T_{\mathrm{B}}\right], & m+\frac{1}{2} \le \frac{t}{T_{\mathrm{B}}} < m+1, \end{cases}$$

where B_{B} and T_{B} are the sweeping bandwidth and period of the triangular waveform, resulting in a sweep rate $\rho = 2B_{\mathrm{B}}f_{\mathrm{B}}$, and $f_{\mathrm{B}} = (T_{\mathrm{B}})^{-1}$ is the sweep frequency. Also, $m = 0, 1, 2, \ldots$ is the index counting the FMCW period. Any other linear FM waveform (e.g., sawtooth) should work with the same principle as we show here, but we choose the triangular waveform since it limits large abrupt changes in frequency that cause high beat frequencies during downconversion.

The FSK modulation is represented in (2) by

$$f_{\mathrm{M}}(t) = \sum_{p=0}^{\infty} \frac{a_p\Delta_{\mathrm{f}}}{2}\mathrm{rect}\left(\frac{t-(p+1)T_{\mathrm{M}}}{T_{\mathrm{M}}}\right), \tag{3}$$

which depends on the FSK symbols $a_p\Delta_{\mathrm{f}}/2$ drawn from a constellation of size M using $a_p \in \alpha_{\mathrm{M}} = \{\pm1, \pm3, \ldots, \pm(M-1)\}$, and whose frequency shift is Δ_{f}. Index p counts the successive symbols with time basis defined by a rectangular function with period T_{M} as in

$$\mathrm{rect}(t) = \begin{cases} 1, & |t| \le 1/2, \\ 0, & \text{otherwise.} \end{cases}$$

The signal received by TRX 1 is

$$y_1(t) = \sum_{k=1}^{K} \beta_k \cos\left[2\pi\left(\varphi_1(t-\tau_k) + \delta_k t\right)\right] \tag{4}$$

$$+ \sum_{l=1}^{L} \gamma_l \cos\left[2\pi\left(\varphi_2(t-\lambda_l) + \delta_l t\right)\right] + z(t), \tag{5}$$

where summations over k and l stand for the Doppler-channel paths from TRX 1 and TRX 2 respectively. These channels have gains β_k and γ_l which account for all amplifications and attenuations in the transmit-receive chains, including antennas and the loss dictated by the basic radar power equation [13]

$$\Gamma_k = \sigma_k / \left(f_{\mathrm{C}}^2(4\pi)^3 R_k^4\right), \tag{6}$$

where σ_k is the kth target's radar cross section (RCS) and R_k is its distance from the transceiver. Path delays τ_k and λ_l are obtained according to $\{\tau_k, \lambda_k\} = 2R_{\{k,l\}}/c$, where c is the speed of light. Additionally, the Doppler shifts δ_k and δ_l in (4), (5) are caused by the target's radial velocity v_k with respect to the static receiver, and they are expressed as $\delta_k = 2v_kf_{\mathrm{C}}$ [13]. Finally, in (5) $z(t)$ is additive white Gaussian noise (AWGN).

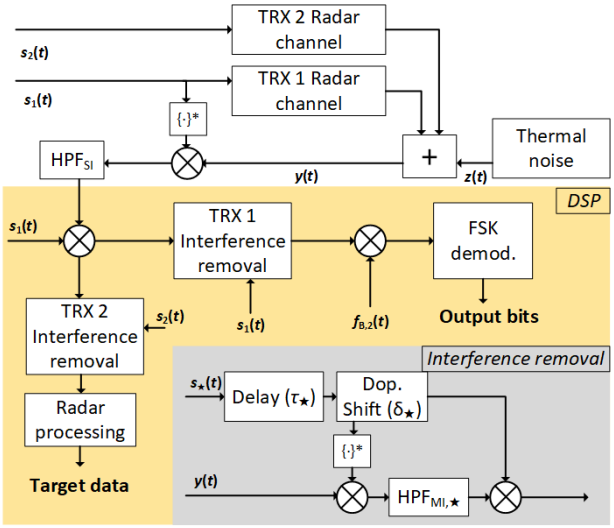

Fig. 2. Block diagram of digital signal processing for TRX 1.

The received signal $y_1(t)$ is then downmixed to complex baseband using the complex conjugate of the transmit waveform (1). Because of this, self-interference (SI) becomes a strong tone at direct current (DC), which is easily suppressed by means of a highpass filter (HPF) labeled as $\mathrm{HPF}_{\mathrm{SI}}\{\cdot\}$ in Fig. 2. However, because the downconversion frequency varies according to (2), baseband signals resulting from this step will move across spectrum in a way influenced by the transmitted FM–FSK tones as well as the beat and Doppler frequencies induced by the targets [11]. Frequency deviations induced by the downmix stage have to be compensated prior to extracting radar and communication information.

B. Signal Processing

The ultimate goal of this setup is to allow ISAC with minimal mutual interference (MI) caused by the other signal present in the shared spectrum, namely TRX 2's signal and its echoes when performing radar processing, and radar returns when demodulating information transmitted by TRX 2.

The block diagram for the signal processing stage can be seen in Fig. 2. The downmixed and SI-free signal is sampled and digitalized. The signal is multiplied with TRX 1's signal, to revert the sweeping effect caused during downconversion, and fed into FSK and radar processing branches.

MI removal is an iterative process done similarly in each branch, and a single iteration can be condensed as

$$\tilde{s}_\star(t) = s_\star(t - \tau_{\{k,l\}})e^{j2\pi\delta_{\{k,l\}}t}, \tag{7}$$

$$\hat{y_1}(t) = \tilde{s}_\star(t)\left[\mathrm{HPF}_{\mathrm{MI},\star}\{y_1(t)\tilde{s}_\star^*(t)\}\right], \tag{8}$$

where $s_\star(t)$ is the known transmitted signal to which we apply delay $\tau_{\{k,l\}}$ and Doppler shift $\delta_{\{k,l\}}$ to replicate either the direct component or a single echo.

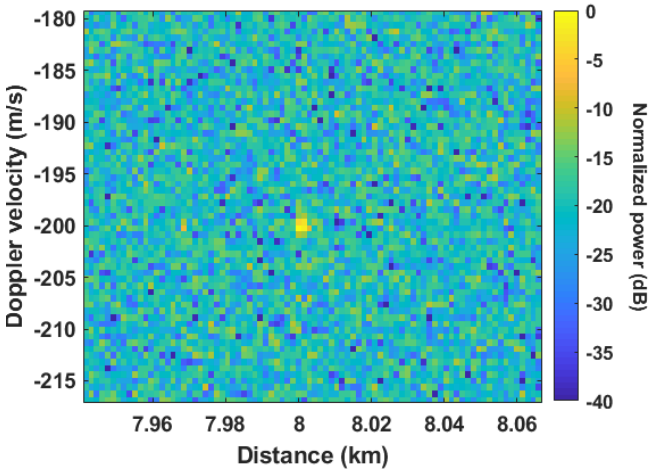

Fig. 3. Simulated range–Doppler result with a radar return from a target at 8 km, with a velocity of −200 m/s and a cross section $\sigma = 10\,\mathrm{m}^2$. The correlation SINR of the echo is 20.9 dB. The power scale has been normalized to the highest correlation power value.

In (8), we multiply the received signal $y_1(t)$ with a conjugate of the replica (7) so the matching MI tone shifts to DC and is filtered out using the $\mathrm{HPF}_{\mathrm{MI},\star}\{\cdot\}$. We then multiply the result again with the component replica, having removed only frequencies occupied by the unwanted MI component. This process is repeated for every unwanted component. Note that in a real setup where the FSK sequence of the TRX 2 might not be known, the replica signal in (7) would only contain the FM sweep without FSK information, which necessitates widening the HPF to also remove random FSK shifts.

Radar processing is based on a standard pulse-Doppler method to retrieve a distance–velocity matrix from the signal with TRX 2's interference removed. The full recording length is divided into shorter pulses which are cross-correlated with the transmitted waveform divided in similar intervals. The results are stored in the columns of a matrix, and a fast Fourier transform (FFT) is applied row-wise to obtain a matrix for which correlation direction denotes the distance and pulse direction the Doppler speed. Targets are identified by means of a threshold operation which contrasts each matrix element with the average correlation value on a square window centered on that element. Fig. 3 shows an example of a range–Doppler processing result with a single radar echo at the center of the figure having 20.9 dB of correlation signal-to-interference-plus-noise ratio (SINR) compared to its surrounding bins.

For demodulating FSK data, we still need to compensate for the spectral sweep in the signal with radar echoes removed. This is done by multiplying this signal with the conjugated replica of TRX 2's FM-sweep signal. Afterwards, FSK information can be easily read by comparing the power levels of the different known symbol frequencies to determine which symbol was sent. These symbols are then mapped to bits according to the used constellation. The bit error rate (BER) can be determined by comparing transmitted and received bits.

TABLE I
DEFAULT SIMULATION PARAMETERS

General	Carrier frequency	f_C	3 GHz
	Sampling frequency	f_S	100 MHz
	Signal length		100 ms
FMCW	Sweep frequency	f_B	3 kHz
	Sweep bandwidth	B_B	80 MHz
	TRX 1 & 2 separation	Δ_F	40 MHz
FSK	Symbol period	T_M	10 µs
	Constellation size	M	16
	Frequency shift	Δ_f	100 kHz
TRX 1	EIRP*		60 dBm
	Antenna isolation		100 dB
TRX 2	EIRP*		23 dBm
	SNR at TRX 1		−10 dB
$\mathrm{HPF}_{\mathrm{SI}}\{\cdot\}$	Stopband width		100 kHz
	Stopband attenuation		200 dB
$\mathrm{HPF}_{\mathrm{MI},\star}\{\cdot\}$	Stopband width		100 kHz
	Stopband attenuation		80 dB
Radar target	Cross section (RCS)	σ_k	$10\,\mathrm{m}^2$
	Distance	R_k	10 km
	Radial velocity	v_k	30 m/s

*Equivalent isotropic radiated power (EIRP)

III. Simulation Results

A. Parameters

Default parameter values used in our simulations can be found in Table I. All signals occupied the same band, however TRX 2 was generated with a starting instantaneous frequency $f_\mathrm{W}(t)$ separated by $\Delta_F = 40\,\mathrm{MHz}$ from the one of TRX 1.

Data bit streams were randomly generated for every simulator run and mapped to the FSK constellation to obtain instantaneous frequencies. Then, the FMCW waveform was added according to (2). The simulator only works with baseband signals (i.e., $f_\mathrm{C} = 0\,\mathrm{Hz}$) and avoids transferring them to radio frequencies (RF) to limit sampling frequency and allow for longer recording lengths. However, the attenuation, Doppler channel effects and thermal noise power levels take into account the system's considered carrier frequency.

The powers of the transmit signals were adjusted to the levels shown in Table I. The direct-path signal from TRX 1 was then attenuated by 100 dB. The channel gains, delays, and Doppler shifts were calculated as shown previously in Section II. These steps were repeated for every radar target. The AWGN signal $z(t)$ is thermal noise at a power level defined by $P_z = k_\mathrm{B} T f_\mathrm{S}$, where k_B is the Boltzmann constant, T is the temperature in degrees Kelvin, and f_S is the sampling frequency, i.e., the double-sided baseband bandwidth. With our default settings, the thermal power level is −94 dBm.

For TRX 2, a direct line-of-sight signal was created by attenuating the transmit signal according to the free-space loss based on the calculated distance to TRX 1, achieving the desired SNR at TRX 1. Radar echoes were generated for TRX 2's signal the same way as for TRX 1. The distance used in (6) is the average between the two transceivers' separation and the two-way distance from TRX 1 to target. This simplified model avoids simulating a 3D environment.

TABLE II
PARAMETER VARIATIONS IN THE SIMULATIONS FOR THE RADAR TARGET, FSK SIGNAL, AND OTHER VARIABLES

Radar target	Distance	R_k	100:100:1000 m, and 1000:500:20000 m
	Velocity	v_k	±200, ±100 and 0 m/s
	RCS	σ_k	1, 10 and 100 m^2
FSK signal	Constellation size	M	2 and 16
	Symbol period	T_M	10 and 100 µs
	SNR (TRX 2)		-30:2:10 dB
Other	Sweep frequency	f_B	1, 5, 10, 15, 20, 40, 60, 80 and 100 kHz
	$HPF_{MI,1}$ & $HPF_{MI,2}$		0, 0.1, 1 and 10 MHz
	Delay error (TRX 2)		-1000:100:1000 samples

SI is removed with an infinite impulse response (IIR) HPF_{SI}, whose stopband is 100 kHz wide and has an ample attenuation of 200 dB. Because of its structure, we have to compensate for the non-uniform group delay to avoid distortions in the filtered signal. Likewise, the $HPF_{MI,1}$ and $HPF_{MI,2}$ used in the signal removal are IIR, and their frequency-selective group delays were also compensated to minimize distortion to the output signals. Their stopband attenuation was set to 80 dB.

Simulations were run with numerous parameter combinations. Each combination was repeated ten times to collect the average radar correlation SINR and FSK BER performance. Table II indicates parameter variations for radar target, FSK signal, and other parameters. Values not specified in result figures are considered equal to the default settings in Table I.

B. Results

Sensing results with different radar target distances, velocities and RCS values can be seen in Fig. 4. We can see that for a very small stationary target ($\sigma_k = 1\,m^2$), the setup can achieve a correlation SINR of 15 dB at approximately 8 km. Targets with RCS equal to 10 and 100 m^2 can be detected at 13 and over 14 km respectively. SINR degrades with increasing target velocity, with 100 m/s causing a few decibel loss and 200 m/s reducing correlation SINR by 5 dB.

Fig. 5 shows how a simulated error in delay estimation, as well as $HPF_{MI,2}$ stopband width can affect radar performance when TRX 2's signal SNR is increased. The results show that without a $HPF_{MI,2}$ the radar performance is very sensitive to TRX 2 interference power. However, with a 1 MHz-wide $HPF_{MI,2}$, only the result with no delay estimation error seems not to degrade performance. With a very wide $HPF_{MI,2}$ of 10 MHz, the delay estimation error seems to have no effect on radar detection, and there appears to be only a minor 1 dB loss to radar correlation SINR from the filtering itself.

In Fig. 6, we can see how the number of symbols, FSK period, $HPF_{MI,2}$ stopband width and FM sweep frequency affect the radar SINR. These parameters have only minor relevance for radar processing, with the exception that at $f_B = 15$, 30, 65, 80 and 100 kHz there are changes to the performance both to the positive and negative directions when a $HPF_{MI,2}$ is attenuating the TRX 2 signal. These anomalies might be caused by how these specific values affect the correlation-based radar processing, while it is certainly peculiar that the $HPF_{MI,2}$ would improve the radar performance.

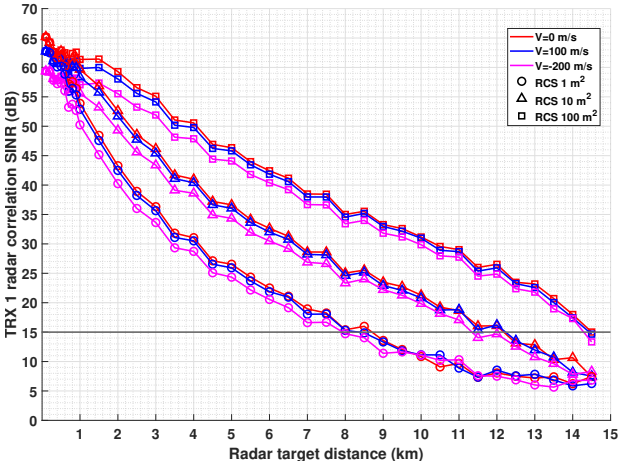

Fig. 4. Effects of radar target distance R_k, velocity v_k and cross section σ_k on the received correlation SINR. A detection threshold of 15 dB is highlighted.

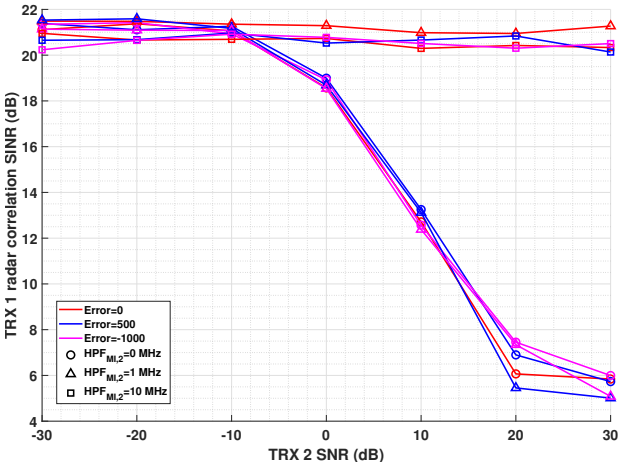

Fig. 5. Effects of TRX 2's SNR, $HPF_{MI,2}$ bandwidth and delay estimation error on radar received correlation SINR.

The FSK performance, while not the main focus in this paper, can be seen in Fig. 7. There the effect of FSK symbol period and number, as well as $HPF_{MI,1}$ width and radar target distance are shown. The RCS of the radar target is 100 m^2. With a shorter 10 µs symbol period, we can see that either without $HPF_{MI,1}$ or with a 10 MHz wide one the reception performance is severely impacted. With a more reasonable 1 MHz $HPF_{MI,1}$, we can see that we can get BER below 1×10^{-3} at SNR below −15 dB for TRX 2's signal. The only exception is the result with $M = 16$, where it seems that the $HPF_{MI,1}$ is not able to completely remove radar echoes and BER raises. By increasing the symbol duration we see that with $T_M = 100$ µs a close-by target can greatly disrupt our reception performance without $HPF_{MI,1}$. However, when adding even a 10 MHz-wide $HPF_{MI,1}$, performance improves dramatically, while reception performance loss is minimal. As a reference, with $M = 16$ and a symbol period of 10 µs, the maximum data transfer rate would be 400 kbit/s.

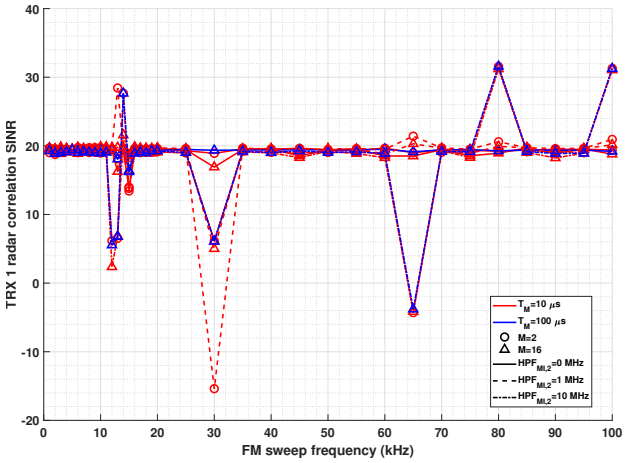

Fig. 6. Effects of FMCW sweep frequency f_{B}, constellation size M, symbol period T_{M} and $\mathrm{HPF}_{\mathrm{MI},2}$ bandwidth on radar correlation SINR.

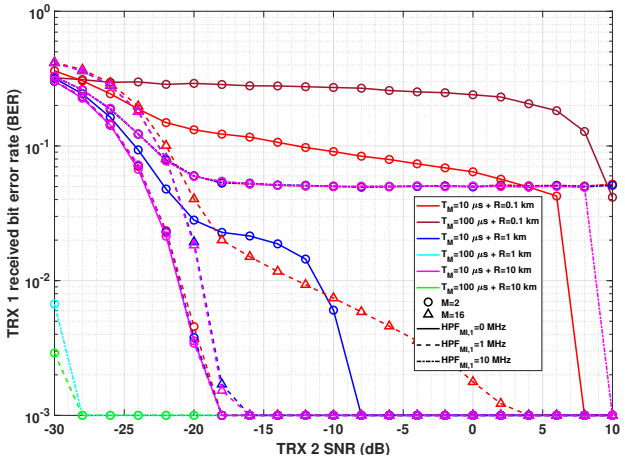

Fig. 7. Effects of target distance R_k, constellation size M, symbol period T_{M} and $\mathrm{HPF}_{\mathrm{MI},1}$ bandwidth on reception BER. Radar cross section is $100\,\mathrm{m}^2$.

IV. Analysis and Discussion

The results in the previous section give us a good idea of how the different parameters affect the radar and FSK-reception performance. We see that radar performance is good as long as we are able to sufficiently reduce the power of the interfering signal from TRX 2. For FSK processing, it is even more crucial to remove radar echoes, especially so when there are nearby reflectors. Furthermore, it is necessary to maintain the HPF bandwidth sufficiently narrow to avoid removing excessive power from the FSK signal itself.

We would like to state that, while the processing presented herein is possible with knowledge of delays, Doppler frequency shifts and FSK symbols perfectly, a real setup would need to estimate the delays and frequency shifts of all the signals with relatively good accuracy for the interference removal operation to work. Furthermore, if we want to use the FSK data to remove the TRX 2 signal for radar processing, we must first decode the FSK symbols, which might require us to already know the radar echo delays. One method to circumvent this paradox would be to only use the a-priori known FM-sweep of the TRX 2 signal to remove that signal in radar processing, however doing so would require a sufficiently wider HPF to also remove the non-compensated FSK shifts. Thankfully, it seems that the radar processing is more robust against the increase of the filter bandwidth.

We believe that our system might be especially interesting for autonomous vehicle use-scenarios, where the relatively low distances would allow for low transmit powers, reducing the interference challenge. Furthermore, the possibility of low-data rate vehicle-to-vehicle communications might further enhance the appeal of using the proposed setup over having separate dedicated sensing and communication devices. Finally, the relatively simple analog self-interference cancelation might be useful in a device-size or cost-constrained environment.

V. Conclusion

We presented through simulated results how well our FM–FSK multipurpose transceiver is capable of performing joint communication and sensing tasks with different parameter combinations. These results demonstrate that our system can detect small targets with RCS of $1\,\mathrm{m}^2$ at 8 km while being able to simultaneously receive and transmit at 400 kbit/s.

References

[1] B. Paul, A. R. Chiriyath, and D. W. Bliss, "Survey of RF communications and sensing convergence research," *IEEE Access*, vol. 5, pp. 252–270, Dec. 2017.

[2] A. Liu *et al.*, "A survey on fundamental limits of integrated sensing and communication," *IEEE Commun. Surveys Tuts.*, vol. 24, no. 2, pp. 994–1034, Feb. 2022.

[3] Y. Cui, F. Liu, X. Jing, and J. Mu, "Integrating sensing and communications for ubiquitous IoT: Applications, trends, and challenges," *IEEE Netw.*, vol. 35, no. 5, pp. 158–167, Sep. 2021.

[4] W. Zhou, R. Zhang, G. Chen, and W. Wu, "Integrated sensing and communication waveform design: A survey," *IEEE Open J. Commun. Soc.*, vol. 3, pp. 1930–1949, Oct. 2022.

[5] M. Kronauge and H. Rohling, "New chirp sequence radar waveform," *IEEE Trans. Aerosp. Electron. Syst.*, vol. 50, no. 4, pp. 2870–2877, Oct. 2014.

[6] G. Dai, L. Zhang, S. Huan, and Z. Wang, "Random stepped-frequency SAR imagery with full cell Doppler coherent processing," *IEEE Geosci. Remote Sens. Lett.*, vol. 19, pp. 1–5, Feb. 2022.

[7] C.-H. Wang and O. Altintas, "Demo: A joint radar and communication system based on commercially available FMCW radar," in *Proc. Vehicular Networking Conference (VNC)*, Dec. 2018.

[8] C. Yang, M. Wang, L. Zheng, and C. Tang, "Dual function system with shared spectrum using FMCW," *IEEE Access*, vol. 6, pp. 79 026–79 038, May 2018.

[9] Z. Xiao and Y. Zeng, "Waveform design and performance analysis for full-duplex integrated sensing and communication," *IEEE J. Sel. Areas Commun.*, vol. 40, no. 6, pp. 1823–1837, Jun. 2022.

[10] C. Baquero Barneto, S. D. Liyanaarachchi, M. Heino, T. Riihonen, and M. Valkama, "Full duplex radio/radar technology: The enabler for advanced joint communication and sensing," *IEEE Wireless Commun.*, vol. 28, no. 1, pp. 82–88, Feb. 2021.

[11] J. Marin, M. Bernhardt, and T. Riihonen, "Full-duplex multifunction transceiver with joint constant envelope transmission and wideband reception," in *Proc. Int. Conf. Acoust., Speech, Signal Process. (ICASSP)*, Jun. 2021.

[12] J. Marin, M. Bernhardt, M. Heino, and T. Riihonen, "Monostatic FMCW radar architecture for multifunction full-duplex radios," in *Proc. 55th Asilomar Conf. Signals, Syst., Comput. (ACSSC)*, Oct. 2021.

[13] M. A. Richards, J. A. Scheer, and W. A. Holm, Eds., *Principles of modern radar: Basic principles*, ser. Electromagnetics and Radar. SciTech Pub., 2010. [Online]. Available: https://books.google.com/books?id=nD7tGAAACAAJ